

Comparative Structure, Oxidation Resistance and Thermal Stability of CoNiCrAlY Overlay Coatings With and Without Pt and Their Performance in Thermal Barrier Coatings on a Ni-Based Superalloy

H. M. Tawancy¹

Received: 25 November 2017 / Revised: 27 December 2017 / Published online: 10 February 2018
© Springer Science+Business Media, LLC, part of Springer Nature 2018

Abstract It is demonstrated that the addition of Pt to CoNiCrAlY overlay coating can significantly improve its oxidation resistance and thermal stability as well as its performance in thermal barrier coatings. The addition of Pt is found to stabilize a surface layer with composition based upon NiAlPt₂ with L1₀ superlattice in addition to enhancing a more favorable distribution of Y and restricting the outward diffusion of detrimental substrate elements particularly Ta and Ti. Due to these beneficial effects, utilizing the Pt-modified bond coating in a TBC system with top coating of zirconia stabilized by yttria is found to extend its lifetime from 410 ± 42 h to 956 ± 48 h as determined from cycling oxidation tests at 1150 °C. However, spallation of the top coatings in the two systems has been correlated with loss of oxide adherence to the bond coatings.

Keywords Oxidation · Superalloys · Bond coatings · Thermal barrier coatings · Electron microscopy

Introduction

MCrAlYs overlay coatings where M stands for Co, Ni or Co + Ni are widely used to maintain the surface integrity of various gas turbine components such as blades, vanes and combustors [1–9], and also as bond coatings in thermal barrier coating (TBC) systems [10–18]. Similar to diffusion aluminides, those coatings rely upon β -phase with NiAl-base composition and cubic B2 superlattice as a source of Al to develop a surface protective layer of Al₂O₃ further improved by the presence of Y

✉ H. M. Tawancy
tawancy@kfupm.edu.sa

¹ Center for Engineering Research, Research Institute, King Fahd University of Petroleum and Minerals, Box 1639, Dhahran 31261, Saudi Arabia

[3, 19–21]. However, the hard and brittle β -phase is embedded in a ductile matrix of solid solution γ -phase, which improves the coating strength under thermal cycling conditions. Compared to diffusion aluminide coatings, although the interaction between the MCrAlY and the superalloy substrate is minimal during coating fabrication, interdiffusion also occurs in service at elevated temperatures, even during post-coating heat treatment. Therefore, in contrast with diffusion-type coatings with performance dependent upon substrate composition, overlays are characterized by more universal applicability.

Since the oxidation resistance of bond coatings is well known to be a key parameter in dictating TBCs lives [22], there is always a need for coatings with superior oxidation properties to meet the demand of engines operating at extreme temperatures exceeding 1000 °C, which requires highly protective oxides based on Al_2O_3 . On the other hand, due to the well-established beneficial effect of platinum on the protective nature of Al_2O_3 several Pt-modified aluminides have been developed and many studies have been devoted to understand the mechanism(s) underlying the beneficial effects of Pt as documented in a review article [23]. However, very few studies have been reported on the influence of Pt on the oxidation resistance of MCrAlYs [24, 25] and the remainder of the studies has focused mostly on the MCrAlYTaN system [26–30]. In one study, it has been argued that Pt has the effect of minimizing the processing defects of the coating [24]. An improvement in isothermal oxidation resistance is reported in another study [25]. Most of the other studies on the Ta-containing MCrAlY have primarily dealt with the Pt-induced structural changes [26–30]. However, no systematic studies have been reported on the oxidation resistance, thermal stability and performance in TBCs utilizing MCrAlYs with and without Pt. Therefore, the present investigation has been carried out to compare the behavior of Pt-modified and Pt-free CoNiCrAlY overlay of commercial grade in terms of oxidation resistance, microstructural stability at high temperatures and behavior in TBC systems using zirconia stabilized by 7 wt% yttria (YSZ) as top coating and the single-crystal superalloy CMSX-4 as substrate.

Experimental Procedures

Table 1 illustrates the nominal composition of superalloy CMSX-4, and the composition of the alloy heat utilized in the present investigation as determined by inductively coupled plasma-atomic emission spectroscopy. The nominal composition of the powder feedstock used to process the CoNiCrAlY overlay is shown in

Table 1 Nominal and actual chemical compositions of superalloy CMSX-4 (wt %)

	Ni	Co	Cr	Ta	W	Al	Re	Ti	Mo	Hf
Nominal	Balance	9	6.5	6.5	6.0	5.6	3.0	1.0	0.6	0.1
Actual	62.49	8.83	6.45	6.39	5.89	5.53	2.86	0.92	0.55	0.09

Table 2 Nominal composition of CoNiCrAlY powder (wt%)

Co	Ni	Cr	Al	Y
38.5	32.0	21.0	8.0	0.5

Table 2. Rods of the alloy (10 cm long and 8 mm diameter) were grit blasted and then ultrasonically cleaned prior to deposition of the overlay coating by vacuum plasma spraying [11]. To determine the effect of Pt addition, a platinum layer with nominal thickness of 7 μm was deposited by wet electroplating [31] on a number of overlay coated samples. One set of samples coated with Pt-free and Pt-modified overlays was heat treated for 3 h at 1150 °C under argon atmosphere as specified for the Pt-free overlay to develop the desired microstructure and reserved for characterization study of the bare bond coatings. In order to develop the coating microstructure and surface film of Al_2O_3 ($\sim 1 \mu\text{m}$ thick) to facilitate the adherence of the top coating, the other set of samples was given the same heat treatment as above in air. Electron beam physical vapor deposition [32] was used to apply the top coating on the Pt-modified coatings with 250- μm -thick layers of zirconia-7 wt% yttria.

The oxidation rates of the bare two bond coatings were characterized by weight change measurements during isothermal exposure in air at 1150 °C. Cycling oxidation tests in air at 1150 °C with air-cooling to room temperature every 24 h were employed to rank the performance of the two bond coatings in the respective TBC systems. Spallation of the top coating was indicative of the TBC lifetime. To reveal the progress of the oxidation reaction at the oxide–bond coating interface, the specimens were subjected to selective deep etching by immersing the specimens for 90 s in 10% bromine—90% methanol etchant followed by ultrasonic cleaning in methanol [33].

Microstructural characterization techniques included scanning electron microscopy (SEM) with microchemical analysis by energy dispersive X-ray spectroscopy (EDS) and wavelength dispersive X-ray spectroscopy (WDS), X-ray diffractometry (XRD) and scanning transmission and transmission electron microscopy (STEM/TEM). To examine the microstructure in the vicinity of the surface of each bond coating at the higher resolution of TEM, foils were thinned by combination of: i) electro-polishing on the alloy side using an electrolyte composed of 30 volume percent nitric acid in methanol and ii) ion beam thinning [34]. The foils were investigated using 200 keV microscope. Henceforth, the NiCrCoAlY coating will be referred to a Pt-free and the NiCrCoAlY + Pt coating will be referred to as Pt-modified.

Experimental Results and Discussion

Initial Microstructures of the Pt-free and Pt-modified Coatings

Typical of the Pt-free overlay, the coating layer consists of colonies of β -phase embedded in a ductile Co-rich solid solution matrix (fcc structure). Figure 1a shows the coating microstructure along the cross section where the 75- μm -thick coating layer is observed with small interdiffusion zone about 6 μm thick and containing particles exhibiting bright contrast with composition approaching that of Ni_4Y in agreement with the results of an earlier study [3]. An X-ray diffraction pattern illustrating the structure of the surface layer is shown in Fig. 1b. All the observed Bragg diffraction peaks are consistently attributed to the β - and γ -phases. The chemical compositions of the β - and γ -phases, and Ni_4Y particles as determined by WDS analysis are listed in Table 3. It is noted that the β -phase is relatively free of Y, which tends to partition to the γ -phase. As shown below, Pt addition is found to cause a significant change in microstructure.

Figure 2 illustrates the microstructure along cross section of the Pt-modified coating as revealed by SEM imaging in the backscattering mode where the average coating thickness is determined to be about 82 μm including an interdiffusion zone about 8 μm in thickness. It is observed that the coating layer is divided into three distinct zones with chemical compositions listed in Table 4 as determined by WDS analysis. The outermost zone marked I is observed to consist of a surface layer of a phase with bright contrast and containing small islands of a phase exhibiting darker contrast. However, as zone II is approached, the structure is changed into a matrix of darker phase containing particles of the brighter phase until the darker phase becomes the sole constituent of zone II. As can be seen, the structure of zone III is the same as that of the Pt-free coating shown in Fig. 1a. Also, the small ID zone

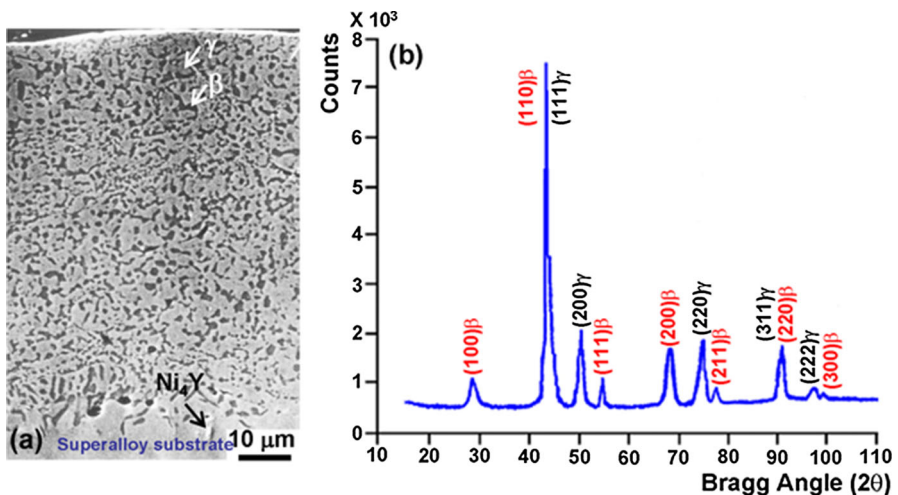


Fig. 1 Initial microstructure of the Pt-free coating. **a** Backscattered SEM image along cross section of the coating. **b** X-ray diffractometer trace derived from the coating surface

Table 3 Composition of CoNiCrAlY coating (at.%)

Phase	Ni	Co	Al	Cr	Y
β	42.93	12.46	35.43	9.18	–
γ	31.98	37.12	8.67	21.60	0.63
Ni ₄ Y	72.89	2.14	3.60	2.43	18.94

Fig. 2 Backscattered SEM image illustrating the microstructure along cross section of the Pt-modified coating

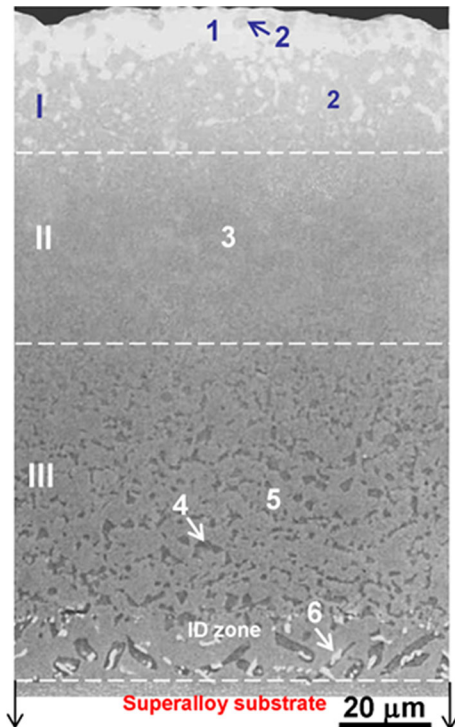


Table 4 Chemical composition of Pt-modified coating in Fig. 2 (at.%)

Zone	Region	Ni	Al	Pt	Co	Cr	W	Ta	Ti	Y
I	1	24.71	21.53	43.24	6.78	3.74	–	–	–	–
	2	27.58	6.73	10.53	25.87	28.99	–	–	–	0.38
II	3	32.07	6.67	5.57	29.64	26.05	–	–	–	–
III	4	44.63	24.15	–	18.04	9.20	–	3.19	0.79	–
	5	43.75	6.88	–	24.03	23.35	1.13	0.76	0.10	–
ID	6	71.65	3.03	–	4.97	2.25	–	–	–	18.10

observed in Fig. 2 resembles that of the Pt-free coating except that it contains higher density of Ni_4Y particles.

Reference to Table 4 shows that the composition of the surface layer with bright contrast (region 1 in Fig. 2) and also the bright particles near zone II closely approaches that of NiAlPt_2 with small concentrations of Co and Cr. This phase has been identified in the ternary Ni–Al–Pt system and designated as τ -phase (face-centered tetragonal structure with L1_0 superlattice) [35]. A further confirmation is provided by the results of TEM/STEM analysis and X-ray diffraction described below. The data of Table 4 indicate that the composition of the phase with darker contrast near the surface (regions marked 2) is consistent with a solid solution with comparable concentrations of Ni and Co and it becomes progressively Ni-rich in zone II (region marked 3). It is also noted from Table 4 that the τ -phase phase is essentially free of Y, which is solely partitioned to the γ -phase near the surface. The compositions of the two phases constituting zone III are observed to be consistent with those of β - and γ -phases (regions marked 4 and 5, respectively); however, in this case the β - and γ -phases become more enriched in Ni as compared to the Pt-free coating (Table 3). It is also shown in Table 4 that the composition of the bright particles (region marked 6) observed in the interdiffusion zone is consistent with that of Ni_4Y similar to the case of Pt-free coating. It is shown later that a one-to-one correspondence appears to exist between the density of Ni_4Y particles near the substrates, and the density and size of Y-rich oxide pegs formed during high temperature oxidation. Due to the higher density of the Ni_4Y particles near the substrate of the Pt-modified coating, less elemental Y is expected to diffuse into the coating surface, which reduces the density and excessive growth of Y-rich oxide pegs. Several studies have shown that internal oxidation is accelerated by higher density and excessive growth of oxide pegs, which in turn reduces the TBC lifetime [20, 25, 36–40]. It is noted here that the present results are in good agreement with

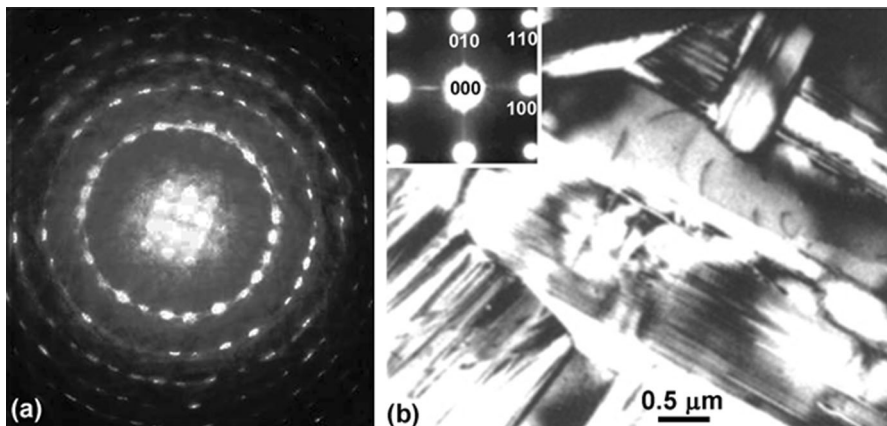


Fig. 3 STEM/TEM analysis of the structure of τ -phase near the surface of the Pt-modified coating. **a** Convergent beam diffraction pattern illustrating the zero and higher order Laue zones. **b** Corresponding STEM bright-field image of the τ -phase; the inset shows the square array of diffraction spots in the zero-order Laue zone and diffuse streaks along the [100] and [001] directions

those reported for an NiCoCrAlYTa bond coating for isothermal oxidation at 1100 °C [26].

The results of analyzing the structure of the τ -phase by STEM/TEM are summarized in Fig. 3. Figure 3a illustrates a convergent beam diffraction pattern derived from the τ -phase. The corresponding bright-field STEM image is shown in Fig. 3b, and the inset shows the zero-order Laue zone with square array of reflections indicative of either a cubic or tetragonal structures viewed along the $\langle 001 \rangle$ direction with $a = b = 0.32$ nm. However, the radii of higher order Laue zones show a lattice parameter of 0.38 nm indicating that the structure is tetragonal rather than cubic. The fine parallel striations observed in Fig. 4b are indicative of the presence of planar imperfections, e.g., twins, stacking faults and anti-phase domain boundaries on the (100) and (010) planes of the τ -phase as indicated by the diffuse streaks observed along the $\langle 100 \rangle$ and $\langle 010 \rangle$ directions in the inset of Fig. 4b. It is noted here that similar defects are reported to exist in the substructure of the NiCoCrAlYTa coating modified by Pt [27].

An example is given in Fig. 4 to illustrate the results of analyzing the τ -phase near the surface of the Pt-modified coating by XRD. A closer look at the microstructure of the τ -phase near the surface is illustrated in Fig. 4a. An X-ray diffractometer trace of the surface is shown in Fig. 4b. In addition to the characteristic fcc reflections, additional reflections characteristic of the τ -phase and in agreement with the results of STEM/STEM analysis described above are also observed in Fig. 4b.

Oxidation Behavior of Bare Coatings

Figure 5 illustrates comparative weight gain by the Pt-free and Pt-modified bare coatings during isothermal oxidation up to 100 h at 1150 °C in still air. It is evident that the addition of Pt has substantially reduced the oxide growth rate. On the other hand, after extended thermal exposure (300 h at 1150 °C), the Pt-free coating is found to experience considerable oxide spallation of the external oxide (Fig. 6a) as well as excessive internal oxidation (Fig. 6b) In contrast, the Pt-modified coating

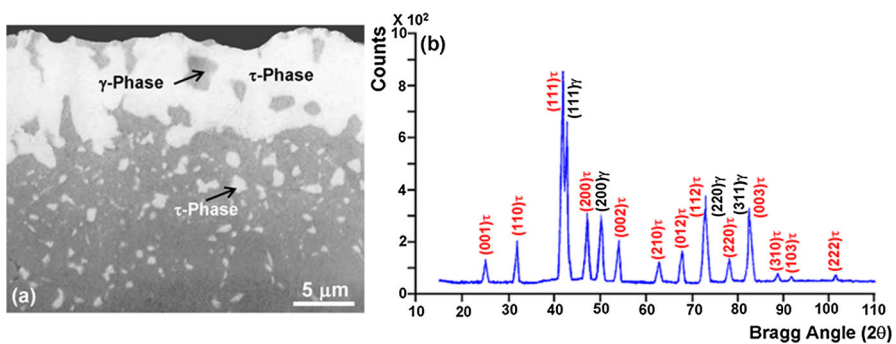


Fig. 4 Analysis of τ -phase by X-ray diffractometry. **a** Backscattered SEM image along the cross section of the Pt-modified coating showing the surface layer of τ - and γ -phases. **b** X-ray diffractometer trace obtained from the surface

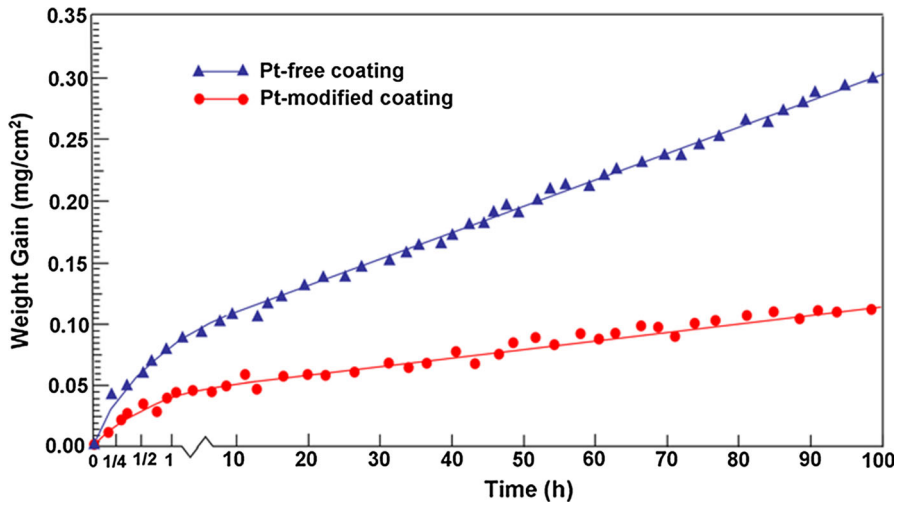


Fig. 5 Comparative oxidation rates of the Pt-free and Pt-modified coatings in the bare condition during isothermal exposure at 1150 °C in air

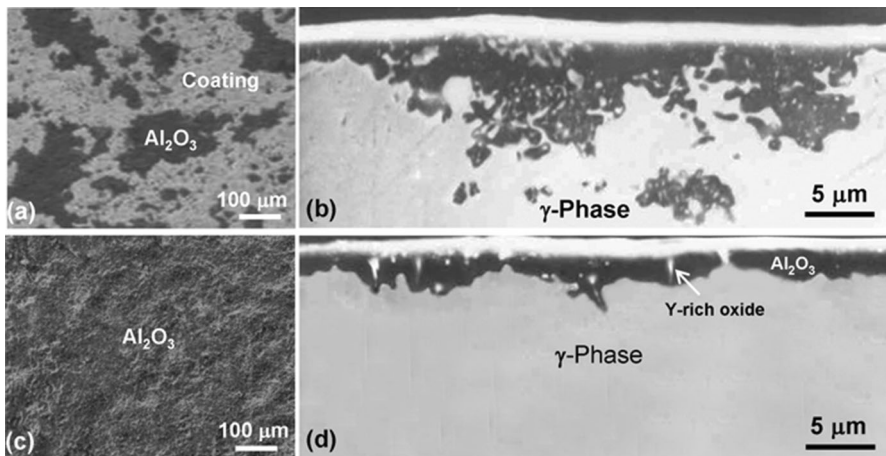


Fig. 6 Secondary electron SEM images illustrating comparative morphologies of the oxides developed by the bare coatings after 300 h of isothermal oxidation at 1150 °C in air. **a** and **b** show, respectively, the surface and cross section morphologies in the Pt-free coating. **c** and **d** show, respectively, the surface and cross section morphologies in the Pt-modified coating

has been able to maintain a continuous layer of protective surface oxide (Fig. 6c) with minimal internal oxidation (Fig. 6d). In both cases, the oxide layer is observed to consist of oxide pegs enriched in Y and dispersed in a matrix of Al₂O₃. However, it is observed that the Y-rich oxide with higher density in the Pt-free coating has penetrated deeper into the coating (Fig. 6b) as compared to the Pt-modified coating (Fig. 6d). This indicates that the presence of Pt has limited the amount of elemental Y, which can reach the surface and be oxidized due to the initial higher density of

Ni₄Y particles near the substrate. The corresponding effect on TBC lives utilizing the Pt-free and Pt-modified bond coatings is elucidated later.

Comparative Thermal Stability

Figure 7 shows the effect of exposure time at 1150 °C on the microstructure of the Pt-free coating. Partial decomposition of the β -phase is observed after 24 h as indicated by the development of surface layer containing a mixture of γ' -phase with Ni₃Al base composition and γ -phase as illustrated in Fig. 7a. Further decomposition of the β -phase is observed with continuous thermal exposure as indicated by thickening of the surface layer free of β -phase (Fig. 7b–d). This behavior can be related to the combined effects of interdiffusion with the superalloy substrate and oxidation, which deplete the surface layers in Al and enrich it in Ni. As a result, the β -phase is transformed into a mixture of γ' -phase and γ -phase (Ni-rich solid solution) as shown in Fig. 7a–c. Eventually, a continuous surface layer of γ -phase is formed after 96 h as shown in Fig. 7d.

In contrast with the Pt-free coating, the Pt-modified coating is found to have higher thermal stability as demonstrated in Fig. 8. It is observed that after 24 h of exposure at 1150 °C (Fig. 8a), the coating microstructure remains quite similar to the initial microstructure prior to thermal exposure (Fig. 2). Also, after 96 h (Fig. 8d), the coating still maintains a Pt-rich layer of τ -phase near the surface. This can explain, at least partially, the difference in oxidation rate of the two coatings shown in Fig. 5. However, another related factor is the difference in density and growth rate of the Y-rich oxide, which can be explained in terms of its initial

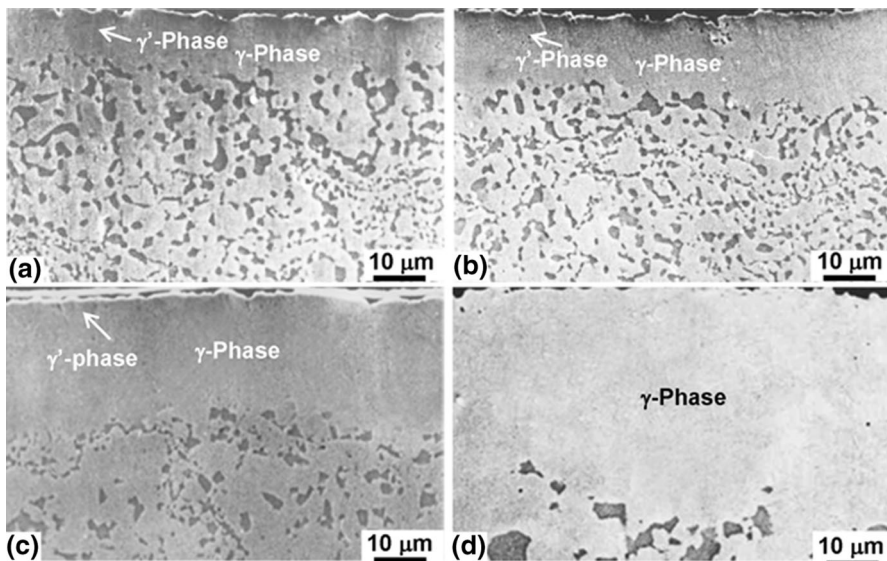


Fig. 7 Backscattered SEM images showing the effect of exposure time at 1150 °C on the microstructure of the bare Pt-free coating. **a** 24 h, **b** 48 h, **c** 72 h, **d** 96 h

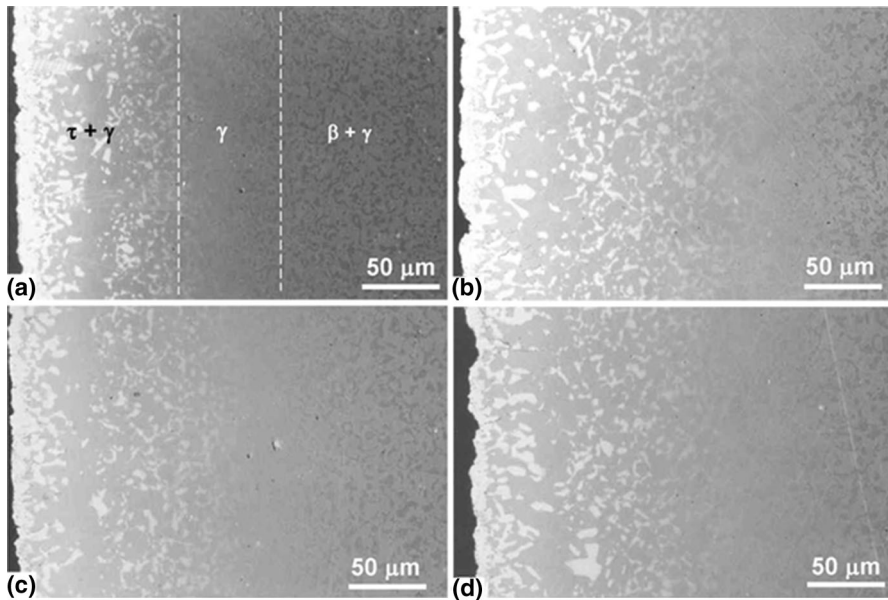


Fig. 8 Backscattered SEM images showing the effect of exposure time at 1150 °C on the microstructure of the bare Pt-modified coating. **a** 24 h, **b** 48 h, **c** 72 h, **d** 96 h

distribution in the two coatings as discussed earlier and corresponding effect on the extent of internal oxidation. In this regard, an earlier study has shown that the size and distribution of Y-rich oxide pegs in the Al_2O_3 oxide developed by a NiCoCrAlYTa overlay are found to have important effect on oxidation kinetics due to differences in the amount of Ni_4Y precipitates near the coating-substrate interface [41]. As shown below, differences between the oxidation resistance and microstructural stability of the two coatings are demonstrated by the variation in their behavior as bond coatings in TBC systems.

Comparative Performance in TBC Systems

Figure 9 illustrates the sequence of events, which take place when a TBC system is exposed at high temperatures. For example, Fig. 9a shows the microstructure along cross section of the TBC system utilizing the Pt-modified coating in the as-deposited condition. Typical of a top coating processed by EBPVD, it consists of columnar grains with boundaries aligned normal to the substrate. The oxide layer intentionally developed during processing is observed between the top coating and bond coating as indicated by the arrow. Figure 9b shows the effect of 576 h of cyclic exposure at 1150 °C, where two changes are observed: i) growth of the initial oxide layer reaching an average thickness of about 4 μm and containing particles of Y-rich oxide, and ii) localized spallation. It is noted here that the actual thermally grown oxide (TGO) is equivalent to the total thickness observed in Fig. 9b minus the initial thickness observed in Fig. 9a. However, the oxide remains well adhered to the

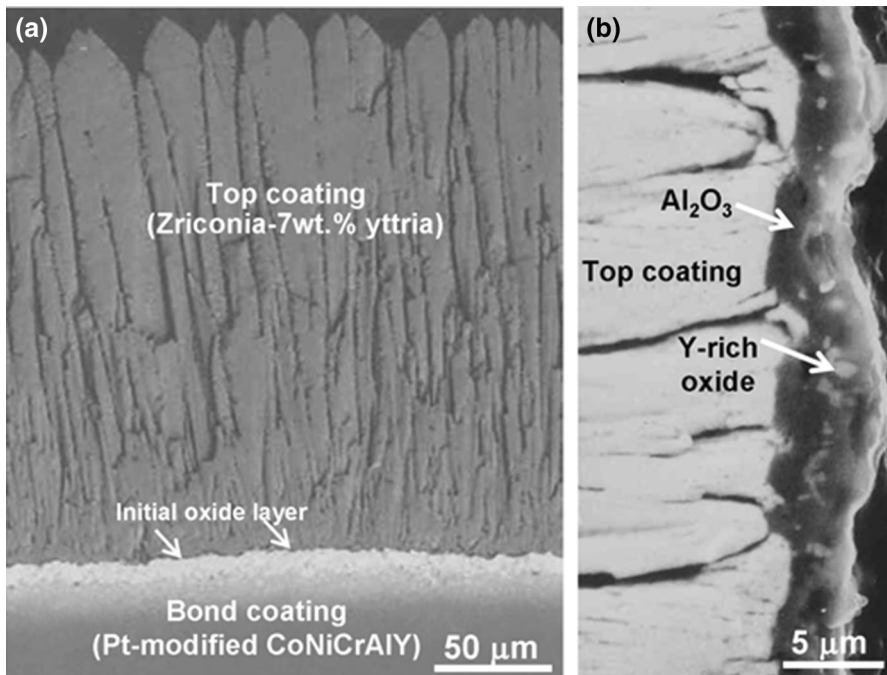


Fig. 9 An example derived from the Pt-modified bond coating to illustrate the sequence of events, which can take place during exposure at 1150 °C with 24-h cycling period to room temperature. **a** Backscattered SEM image illustrating the initial microstructure along cross section of the top coating and into the initial oxide layer and underlying bond coating. **b** Backscattered SEM image along the cross section illustrating the effect of 576 h of cyclic exposure where oxide growth and localized spallation are observed

bottom surface of the top coating (Fig. 9b) indicating that the interface between the oxide and bond coating represents the weakest link in the TBC system. On the other hand, it is emphasized that changes such as those shown in Fig. 9b do not occur homogeneously. In other words, specific processes occur at various locations after different times.

In all experiments, spallation of the top coating has been observed to occur upon cooling and particularly near room temperature. This indicates that the strain energy stored in the oxide as a result of the growth stresses and thermal expansion mismatch at the oxide–bond coating interface provides the driving force for spallation [22]. Based upon the data obtained from testing 12 specimens from each TBC system, the lifetime of the TBC system with the Pt-modified bond coating has been determined to be 956 ± 48 h as compared to 410 ± 42 h for the system utilizing the Pt-free coating (Fig. 10). This substantial difference in TBC lifetime is correlated with the behavior of each bond coating as described below.

Consistent with the results of weight change measurements shown in Fig. 5 (bare coatings), Fig. 11 shows that the TGO on the Pt-modified coating is thickened at considerably slower rate in comparison with the Pt-free coating. Also, consistent with the tendency for internal oxidation shown in Fig. 7 (bare coatings), the growth of the Y-rich oxide pegs in the TGO developed by the Pt-modified coating during

Fig. 10 Comparative lifetimes of the TBC systems utilizing the Pt-free and Pt-modified bond coatings as determined from oxidations tests at 1150 °C with 24-h cycling period to room temperature

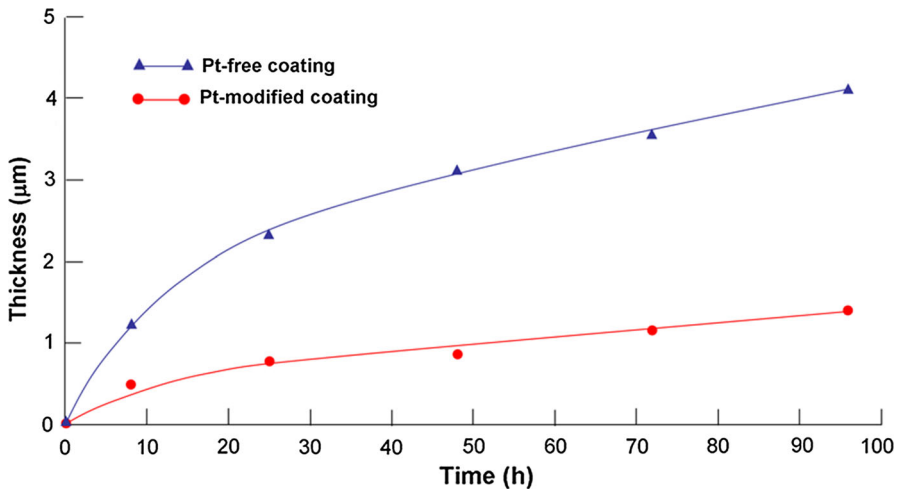
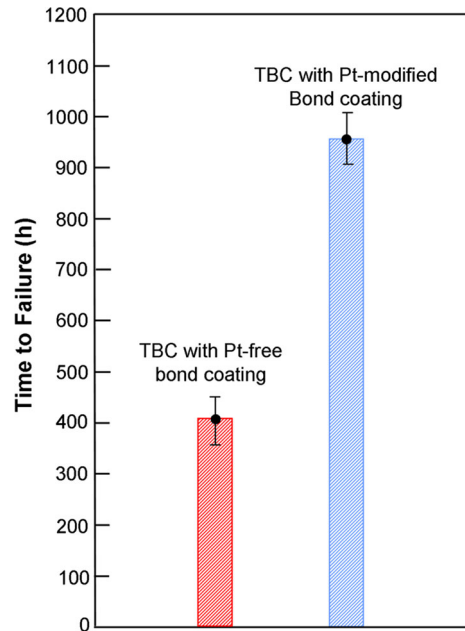


Fig. 11 Comparative thickening rates of the thermally grown oxide on the Pt-free and Pt-modified coatings as functions of cyclic exposure time at 1150 °C in air (total thickness–initial thickness)

cyclic oxidation at 1150 °C as revealed by selective deep etching is observed to occur at a slower rate with smaller density as shown in Fig. 12. In contrast, excessive growth and higher density of oxide pegs are observed at earlier stages of cyclic oxidation as illustrated in Fig. 13.

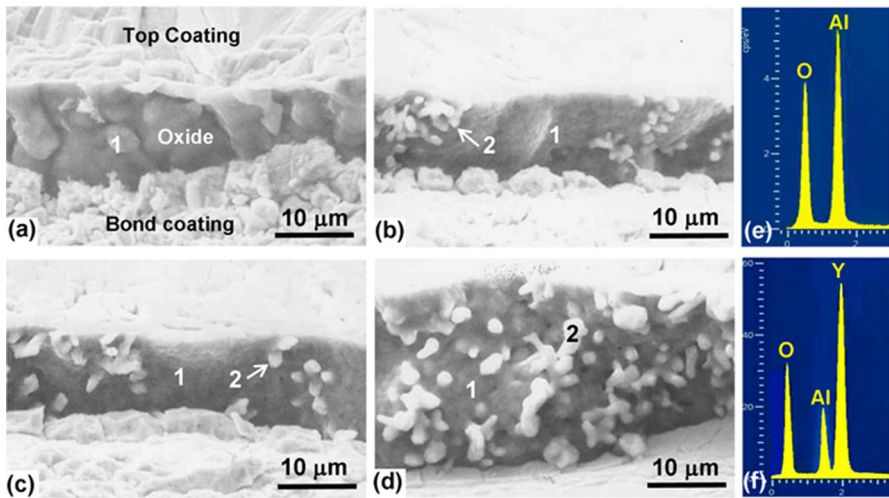


Fig. 12 Secondary electron SEM images and corresponding EDS spectra illustrating the morphology and composition of the interfacial thermally grown oxide on the Pt-modified coating as function of cyclic exposure time at 1150 °C and as revealed by selective deep etching. **a** 24 h, **b** 96 h, **c** 144 h, **d** 360 h, **e** EDS spectrum representative of the regions marked 1 in (a–c). **f** EDS spectrum representative of the regions marked 2 in (a–c)

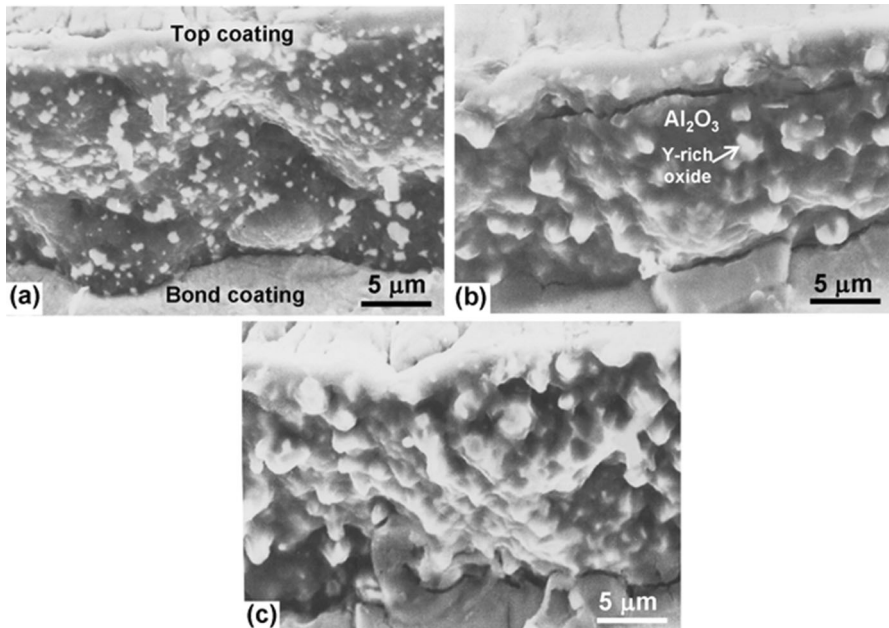


Fig. 13 Secondary electron SEM images illustrating the morphology of the interfacial thermally grown oxide on the Pt-free coating as a function of cyclic exposure time at 1150 °C as revealed by selective deep etching. **a** 24 h, **b** 72 h, **c** 120 h

Despite the observed differences in the properties of the Pt-free and Pt-modified coatings, failure of the respective TBC systems is found to occur by decohesion of the TGO leading to spallation of the top coating. An example obtained from the TBC system utilizing the Pt-free bond coating is shown in Fig. 14. Figure 14a, b shows, respectively, the morphological features of the bond coating surface and bottom surface of the top coating exposed by TBC failure in a specimen cycled 256 h at 1150 °C. Figure 14c shows an EDS spectrum illustrating the elemental constituents of the bond coating surface (region 1 in Fig. 14a). Internal oxidation is reflected by the observation of large islands consisting of Al_2O_3 (regions marked 2 in Fig. 14a) and containing particles of Y-rich oxide (region 3 in Fig. 14a) as indicated by the EDS spectra of Fig. 14d, e, respectively. In addition, voids containing particles of Ta, Ti-rich oxide are also observed at the bond coating surface (regions 4 in Fig. 14a) as shown in the EDS spectrum of Fig. 14f. The same types of oxides are observed at the bottom surface of the top coating (Fig. 14b) as indicated by the regions marked 2 (Al_2O_3 matrix layer), 3 (Y-rich oxides) and 4 (Ta, Ti-rich oxide).

A qualitatively similar behavior to that described above is found to occur in the TBC system using the Pt-modified bond coating as illustrated in the example of Fig. 15, which is derived from a specimen cycled 768 h at 1150 °C. Figure 15a, b illustrates the morphology of the bond coating surface (same region observed at different magnifications). An island of Al_2O_3 is observed to contain Y-rich oxide particles in addition to small voids containing Ta, Ti-rich oxide particles as marked in Fig. 15b. The morphology of the bottom surface of the top coating is shown in

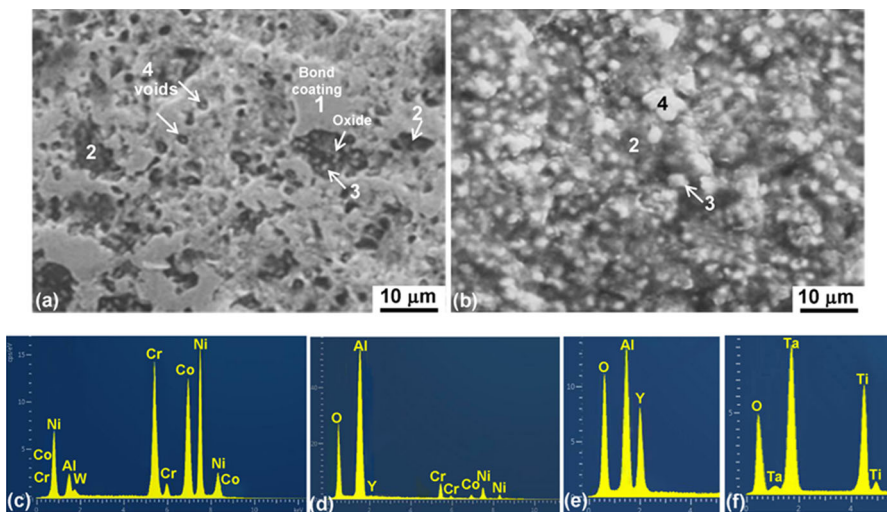


Fig. 14 Analysis of the surfaces exposed by spallation of the top coating in the TBC system utilizing the Pt-free coating (specimen cycled 256 h at 1150 °C). **a** and **b** are secondary electron SEM images illustrating the morphologies of the bond coating surface and bottom surface of the top coating, respectively. **c–f** are EDS spectra illustrating, respectively, the elemental compositions of the bond coating surface (region 1 in **a**), Al_2O_3 (regions 2 in **a–b**), Y-rich oxide (regions 3 in **a** and **b**) and Ta, Ti-rich oxide (regions 4 in **a** and **b**)

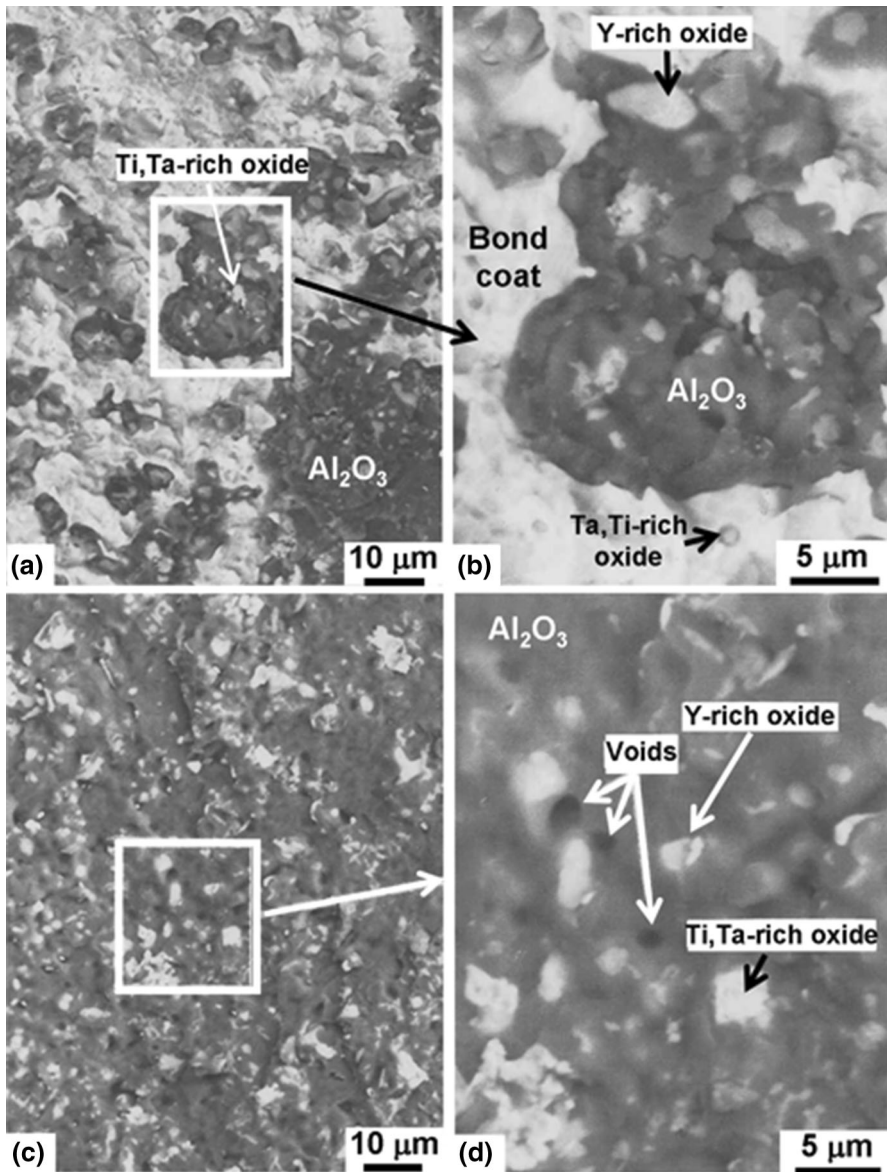


Fig. 15 Analysis of the surfaces exposed by spallation of the top coating in the TBC system utilizing the Pt-modified coating (specimen cycled 768 h at 1150 °C). **a** and **b** are secondary electron SEM images illustrating the morphology of the exposed bond coating surface as viewed at different magnifications; an island of Al₂O₃ containing particles of Y-rich oxide and Ta, Ti-rich oxide is observed. **c** and **d** are secondary electron SEM images illustrating the morphology of the exposed bottom surface of the top coating as viewed at different magnifications; voids and particles of Y-rich oxide and Ta, Ti-rich oxide are observed in the layer of Al₂O₃

Fig. 15c, d as viewed at different magnifications. Particles of Y-rich oxide, voids and particles of Ta, Ti-rich oxide are observed in the Al_2O_3 layer as indicated in Fig. 15d.

The above observations indicate that the benefits gained from the addition of Pt to the bond coating stem from slowing down the processes leading to the failure of the TBC system by improving the oxidation resistance and thermal stability involving more favorable distribution of Y and restricting the outward diffusion of detrimental substrate elements particularly Ta and Ti. On the other hand, the above observations also indicate that spallation of the top coating in both TBC systems is triggered by formation and coalescence of voids around Ta, Ti-rich oxide and fracture of the Y-rich oxides at the thermally grown oxide–bond coating interface.

Conclusion

The addition of Pt to CoNiCrAlY overlay bond coating is found to extend the TBC lifetime by more than twofold relative to the Pt-free bond coating. The beneficial effect of Pt is correlated with significant improvement in oxidation resistance and thermal stability due to the formation of surface layer based upon the NiAlPt_2 composition. However, the oxide–bond coating interface is identified as the weakest link in the TBC systems utilizing the Pt-free and Pt-modified bond coatings leading to the same failure mechanism. The results indicate that the overall role of Pt is to slow down the processes leading to failure of the TBC system, which include higher density and excessive growth of Y-rich oxide pegs and formation of voids around Ta, Ti-rich oxide particles at the TGO–bond coating interface.

Acknowledgements The author is most grateful for the continued support provided by King Fahd University of Petroleum and Minerals.

References

1. B. H. Kear and E. R. Thompson, *Science* **208**, 847–856 (1980).
2. R. Sivakumar and B. L. Mordike, *Surface and Coatings Technology* **37**, 139–160 (1989).
3. H. M. Tawancy, N. M. Abbas and A. Bennett, *Surface and Coatings Technology* **68**, (69), 10–16 (1994).
4. W. Brandl, H. J. Grabke, D. Toma and J. Kruger, *Surface and Coatings Technology* **86**, (87), 41–47 (1996).
5. M. J. Pomeroy, *Materials and Design* **26**, 223–231 (2005).
6. S. Bose, *High Temperature Coatings, Chapter 6*, (Elsevier, Amsterdam, 2007).
7. A. Gil, V. Shemet, R. Vassen, M. Subanovic, J. Toscano, D. Naumenko, L. Singheiser and W. J. Quadakkers, *Surface and Coatings Technology* **201**, 3824–3828 (2006).
8. W. G. Sloof and T. J. Nijdam, *International Journal of Materials Research* **100**, 1318–1330 (2009).
9. M. T. Pace, R. C. Thomson and J. Wells, in *Superalloys 2008*, eds. R. C. Reed, K. A. Green, P. Caron, T. P. Gabb, M. G. Fahrman, E. S. Huron and E. S. Woodward (The Minerals, Metals and Materials Society, Warrendale, Pennsylvania, 2008), pp. 651–660.
10. C. Nordhom, R. Mucke, K. A. Unocic, M. J. Lance, B. A. Pint and R. Vassen, *Surface and Coatings Technology* **258**, 608–614 (2014).
11. C. U. Hardwicke and Y.-C. Lau, *Journal of Thermal Spray Technology* **22**, 564–576 (2013).
12. R. D. Jackson, M. P. Taylor, H. E. Evans and X.-H. Li, *Oxidation of Metals* **76**, 259–271 (2011).

13. A. Feuerstein, J. Knapp, T. Taylor, A. Ashary, A. Bolcavage and N. Hitchman, *Journal of Thermal Spray Technology* **17**, 199–213 (2007).
14. B. Gleeson, *Journal of Propulsion and Power* **22**, 375–383 (2006).
15. N. P. Padture, M. Gell and E. H. Jordan, *Science* **296**, 280–284 (2002).
16. A. G. Evans, D. R. Mumm, J. W. Hutchinson, G. H. Meier and F. S. Pettit, *Progress in Materials Science* **46**, 505–556 (2001).
17. H. M. Tawancy, N. Sridhar, N. M. Abbas and D. S. Rickerby, *Journal of Materials Science* **35**, 3615–3629 (2000).
18. J. Nicholls, *JOM* **52**, 28–35 (2000).
19. H. M. Tawancy, *Oxidation of Metals* **86**, 371–383 (2016).
20. H. Hindam and D. P. Whittle, *Oxidation of metals* **18**, 245–284 (1982).
21. A. M. Huntz, in *The Role of Active Elements in the Oxidation Behavior of High-Temperature*, ed. E. Lang (Elsevier, Amsterdam, 1989), pp. 81–110.
22. H. E. Evans, *Surface and Coatings Technology* **206**, 1512–1521 (2011).
23. D. K. Das, *Progress in Materials Science* **58**, 151–182 (2013).
24. N. M. Yanar, G. H. Meier and F. S. Pettit, *Scripta Materialia* **46**, 325–330 (2002).
25. D. Joo, S. Park, Y. Jung, J. Lee, C. Ye and K. Lee, *Materials Science Forum* **544–545**, 721–724 (2007).
26. A. V. Put, D. Oquab, E. Pe're', A. Raffaitin and D. Monceau, *Oxidation of Metals* **75**, 247–279 (2011).
27. X. Tan, C. Pellegrino, K. Hoummada, D. Mangelinck, A. Put, M. Lafont, D. Oquab and D. Monceau, *Corrosion Science* **76**, 1–5 (2013).
28. A. V. Put, M. Lafont, D. Oquab, A. Raffaitin and D. Monceau, *Surface and Coatings Technology* **205**, 717–727 (2010).
29. D. Monceau, D. Oquab, C. Estournes, M. Boidot, S. Selezneff and N. Ramond, *Materials Science Forum* **654–656**, 1826–1831 (2010).
30. D. Monceau, D. Oquab, C. Estournes, M. Boidot, S. Selezneff, Y. Thebault and Y. Cadoret, *MCrAlY-base multilayer coatings and TBC systems fabricated by spark plasma sintering for the protection of Ni-base superalloys*, *Surface Coatings and Technology* **204**, 771–778 (2009).
31. C. R. K. Rao and D. C. Trivedi, *Coordination Chemistry Reviews* **249**, 613–631 (2005).
32. H. Lammermann and G. Kienel, *Advanced Materials and Processes* **140**, 18–23 (1991).
33. H. M. Tawancy, *Metallography, Microstructure and Analysis* **2**, 88–95 (2013).
34. P. J. Goodhew, J. Humphreys and R. Beanland, *Electron Microscopy and Analysis*, 3rd ed, (Taylor and Francis, New York, 2002), pp. 24–27.
35. V. Raghavan, *Journal of Phase Equilibria and Diffusion* **32**, 64–66 (2011).
36. R. Pendse and J. Stringer, *Oxidation of Metals* **23**, 1–16 (1985).
37. H. Guo, L. Sun, H. Li and S. Gong, *Thin Solid Films* **516**, 5732–5735 (2008).
38. J. Toscano, R. Vaben, A. Gil, M. Subanovic, D. Naumenko, L. Singheiser and W. J. Quadackers, *Surface and Coatings Technology* **201**, 3906–3910 (2006).
39. H. Lau, C. Leyens, U. Schulz and C. Friedrich, *Surface and Coatings Technology* **165**, 217–223 (2003).
40. G. Fisher, P. K. Datta, J. S. Burnell-Gray, W. Y. Chan and J. C. Soares, *Surface and Coatings Technology* **110**, 24–30 (1998).
41. T. J. Nijdam and W. G. Sloof, *Oxidation of Metals* **69**, 1–12 (2008).